A coupled, pore-scale model for methanogenic microbial activity in underground hydrogen storage

Anozie Ebigbo [a,*], Fabrice Golfier [a], Michel Quintard [b,c]

[a] Université de Lorraine, ENSG; CNRS; CREGU; GeoRessources UMR 7359, 54518 Vandœuvre-lès-Nancy Cedex, France
[b] Université de Toulouse; INPT, UPS; IMFT (Institut de Mécanique des Fluides de Toulouse), Allée Camille Soula, F-31400 Toulouse, France
[c] CNRS; IMFT; F-31400 Toulouse, France

Keywords:
Underground hydrogen storage
Coupled model
Methanogenesis
Biofilm
Pore-scale simulation

A B S T R A C T

Underground hydrogen storage (UHS) as a means of energy storage is an efficient way of compensating for seasonal fluctuations in the availability of energy. One important factor which influences this technology is the activity of methanogenic microorganisms capable of utilising hydrogen and carbon dioxide for metabolism and leading to a change in the stored gas composition. A coupled, pore-scale model is presented which aids in the investigation of the mechanisms that govern the conversion of hydrogen to methane, i.e. advective hydrogen flow, its diffusion into microbial biofilms of multiple species, and its consumption within these biofilms. The model assumes that spherical grains are coated by a film of residual water and treats the biofilm development within each film in a quasi one-dimensional manner. A sample simulation using the presented model illustrates the biofilm growth process in these films as well as the competition between three different microbial species: methanogens, acetogens, and acetotrophs.

1. Introduction

1.1. Underground storage of hydrogen

Increasing energy demand and anthropogenic greenhouse-gas emissions pose serious challenges for national and international energy economies. Low emissions and the increasing efficiency of fuel cells make the case for the use of hydrogen (H_2) as *the* fuel of the future [1,2]. At best, H_2 is generated, e.g. through electrolysis, from renewable energy sources. In such a scheme, storing H_2 comes down to storing electricity. However, it may also be produced from fossil fuels, making it easier to contain emissions at the power plants while distributing clean energy in form of H_2, e.g. for transportation.

Obviously, variations in the supply of and demand for energy inadvertently lead to the need for appropriate storage solutions (in this case, in the form of H_2) on a large scale. Even though various forms of storage exist, the underground storage of H_2 has been found to be among the cheapest at the scale of interest [1,3]. This may be in depleted oil or gas fields, aquifers, or underground caverns (rock or salt) [1,4]. Note, however, that the present study focuses on storage in porous reservoirs (mainly deep aquifers) and on the technology-related issues. Owing to the high mobility of H_2 (low density, low viscosity, high diffusivity), storage operations typically have to deal with the problem of loss due to leakage. It is important to differentiate underground hydrogen storage (UHS), the temporary storage of a fuel, from carbon capture and storage (CCS), the disposal of a waste product. UHS is faced with more severe leakage problems, and very importantly, there is a potential for the consumption of stored H_2 due to microbial activity [5]. Note that increased attention has recently been paid to abiotic hydrogen reactivity at low temperatures [6] which could impact H_2 storage, but such geochemical aspects will not be considered here.

In natural subsurface environments, several microorganisms are active, even at great depths [7,8]. The type of microbial activity which dominates in a given region or at a given depth often depends on the terminal electron acceptor available, e.g. iron (III), sulphate, carbon dioxide. Specialised microorganisms (methanogens) are capable of using carbon dioxide (CO_2) as the terminal electron acceptor to consume H_2. Due to extremely low H_2 concentrations in the subsurface, such hydrogenotrophic activity tends to be very slow. However, in a UHS site, there is an abundance of H_2 in the residual water. If the stored gas contains CO_2, as is the case for town gas, the same goes for dissolved CO_2. Šmigáň et al. [9] and Buzek et al. [10] report significant changes in the composition of stored town gas (less H_2 and CO_2, and more methane, CH_4) caused by microbial activity. However, due to the novelty of this research topic, the published literature is still very poor and consists mostly of an inventory of geological structures suitable for hydrogen storage [11] or studies on technology-related issues [12,13] and the

* Corresponding author. Tel.: +49 241 80 49882; fax: +49 241 80 49889.
E-mail addresses: ebigbo@gmail.com, AEbigbo@eonerc.rwth-aachen.de (A. Ebigbo).

hydrodynamic behaviour of the gas [14]. Though a few multiphase transport models have recently been derived to investigate the coupling with bacterial population dynamics see an application of such a model to CO_2 storage in [15], the coupled mathematical model proposed by Panfilov [5] is, to the best of our knowledge, the only one that considers the impact of hydrogenotrophic activity in such a UHS site at the macroscopic scale. Due to its applicability on the reservoir scale, the model is highly relevant. It can, however, be improved by tackling its simplistic description of the biological processes (single bacterial species, homogeneous distribution of the biofilm within the fluid phase) and lack of information on effective growth and degradation rates.

Even though some information on conversion rates by methanogenic microbial cells exists, it is not clear how colonies of microbes interact to produce an effective conversion rate, how various microbial strains compete for H_2 within biofilms, or which processes and mechanisms dominate at the various scales. This research gap motivates the present work at the pore scale. It is the goal of this study to develop a numerical model which can help answer these questions, contribute towards the general understanding of how microbial processes affect UHS, and ultimately aid in quantifying effective rate parameters of H_2 conversion at the reservoir scale.

1.2. Coupled models at the pore scale

The development of coupled models for groundwater flow and transport, microbial activity, and biofilm growth has a long history from an environmental and engineering perspective. Describing bacterial-cell proliferation in biofilms poses special challenges to mathematical models. The interface between the biofilm and the bulk water tends to be sharp, leading to a discontinuous distribution of microbial activity. There is an extensive literature on this subject, and a recent review and classification of such mathematical models at the biofilm and/or pore scale can be found in [16]. Biofilm models may roughly be divided into several categories including discrete-continuum/cellular-automaton models (e.g. [17]), continuum models (e.g. [18]), and individual-based models (e.g. [19]), with each class of models having its own set of strengths and drawbacks. Since the pioneering work of [20], pore-scale models of biofilm formation have become increasingly complex, starting with a single pore [21] to the first porous systems [22]. However, even though they proved their capability of modelling the various biofilm morphologies, they remain limited to two-dimensional geometries [23] or small volumes of interest [24]. Moreover, up to now, no model has investigated these aspects for two-phase conditions. From this brief state of the art of ongoing research and keeping in mind our ultimate goal to be addressed in this work (i.e. determining dominant mechanisms and conversion rates in a representative elementary volume), the issues mentioned above call for a description of processes on *both* the biofilm and pore scales.

In studying flow and transport processes involving microbial activity in the subsurface, indeed, several characteristic length scales can be identified [25,26], ranging from the microbial-cell scale, the biofilm scale, the pore scale, the Darcy scale, up to the field/reservoir scale. In our case, the methanogenic reactions take place in the presence of microbial cells which accumulate in the biofilm while the flow and transport of the various gases occur at the pore scale. As stated by Eberhard et al. [27], biofilm processes can be resolved using length scales of micrometres and time scales of hours to days. Pore-scale flow and transport processes, however, can be resolved using length scales of millimetres and time scales of seconds to minutes. Such a disparity of scales in time and space makes it impracticable to consider pore-scale simulations over a large volume with complete microbial-scale resolution.

The classical way of addressing this issue would be to apply some form of upscaling. This has been done successfully in the past for different problems related to microbiological processes in porous media [26,28–30]. However, the underlying approximations and assumptions may not be justified, especially when strong coupling exists between both scales, leading to a breakdown of the model (see a discussion on the validity domains of continuum transport models in [29]). For instance, assuming local mass equilibrium between water and biofilm phases, an upscaling of the complicated biofilm-scale processes involved in a UHS reservoir would give a two-phase system (the gas phase and a pseudo-reactive water phase) at the pore scale. The effective reaction term associated with the water-film layer could be computed from a closure problem using a unit cell as complex as necessary to capture the biofilm geometry. However, changes in time of this coefficient due to the path dependence of the processes (e.g. biofilm growth and decay) would be lost in such an approach. This difficulty is indeed well known for systems with process-dependent, evolving geometries. In general, there is no simple, direct relationship between a macro-scale transport property and a single macro-scale geometrical characteristic, e.g. a volume fraction, as traditionally used in macro-scale models.

Alternatively, one may keep the scales of the different processes if appropriate coupling methods exist see a recent review of such coupling methods in [31,32]. When used appropriately, they are capable of simulating relatively complex multi-scale processes in a computationally efficient manner [32–34].

In this work, biofilm-scale processes (biomass growth, H_2 consumption) are coupled to the pore-scale processes (gas flow and transport) via a mass exchange term and appropriate boundary conditions. Such an approach is used in a similar way by Eberhard et al. [27] for less complex problems (single fluid phase, mono-species biofilm).

2. Conceptual pore-scale model

A conceptual model which describes the flow of gases through the pores of a porous medium, the growth of biofilms on water-coated grains, and the microbial consumption and production of the dissolved gases – as they pertain to the storage of H_2 in the subsurface – is presented here.

To the authors' knowledge, no model is currently able to account fully and comprehensively for the coupling between two-phase flow with evolving interfaces, reactive species transport and microbial activity in a complex pore-scale geometry. This is a very first attempt to tackle such a complex problem. Obviously, dealing with this complexity requires a series of simplifying assumptions which are listed below:

- The considered region is far from the injection point. The Reynolds numbers are much less than one ($Re \ll 1$).
- A H_2–CO_2–CH_4 gas mixture flows through a porous medium which is residually saturated with water. At this point in time, the gas phase has displaced all mobile water. Achieving a low water saturation in a relatively high-porosity medium is indeed a technical goal for such underground storage.
- Any variations in the properties or geometry of the gas–water interface as a result of biofilm activity, e.g. as observed on the Darcy scale by Rockhold et al. [35], are considered to be small and neglected. In a similar way, any potential impacts generated by aqueous films due to surface tension on bacterial motility and biofilm growth [36] are discarded.
- The porous medium is composed of spherically shaped grains which are coated with a layer of water, i.e. a water film. This is a crude simplification of a real porous-medium geometry

intended for easy implementation of this screening study. It should be clearly stated that residual water in a porous medium can have a very heterogeneous distribution [37], accumulating at grain contact points, i.e. pendular rings, and in films. Hence, assuming the water is uniformly distributed around the grains is an approximation. Given the error made on the geometry, as compared to a real porous medium and the fact that it has been observed that the water–gas interfacial area is often on the order of the solid surface interfacial area for unconsolidated porous media [37], it is reasonable to neglect, for our simplified system, the pendular-ring effects and assume that water films are predominant.

- Microbial cells may form biofilms within the layer of water on the grains and consume/produce dissolved gases, which would lead to further dissolution of gases from (or exsolution to) the gas phase. At the grain scale, biofilm heterogeneity is assumed to be negligible.
- The geometry and other characteristics of the grains and water film call for a radial treatment of the boundary condition. Under the assumption that the gas Péclet numbers are small, which is compatible with the problem under consideration, the concentrations over the gas–water interface may be taken as uniform, allowing for a spherical symmetry of all unknown variables. Therefore, microbial growth and activity within the water film is assumed to be spherically symmetric around the centre of the grain.
- The exchange of components between the water and the gas phases is entirely driven by diffusion.
- CO_2 is assumed to be the sole electron acceptor available for microorganisms. In reservoirs containing significant amounts of sulphates or iron, these may also serve as electron acceptors. However, the CO_2-utilising microbial species can consume H_2 regardless of the mineral composition [8].
- Reactions involving the solid mineral phase (e.g. dissolution, precipitation) are neglected. Hence, potential effects that dissolved CO_2 may have on the mineral phase are not accounted for.

The disparity of scales and processes is summarised in Fig. 1. As can be seen in the figure, the biofilm growth within the water film and the gas flow through the porous medium need to be properly modelled. In the following sections, appropriate models for the biofilm (Section 2.1) and gas flow (Section 2.2) are presented in a general manner. Section 2.3 proposes a coupled scheme which relates these two models while retaining their respective scales of interest.

2.1. Biofilm model

The biomass accumulation and microbial activity in the film of water, which is assumed to coat each grain, is described in this section. The relevant organisms are identified and their activity quantified with kinetic rates within the framework of a continuum biofilm model.

2.1.1. Microbial reactions

Subsurface microorganisms tend to exist predominantly as groups of cells attached to solid surfaces and held together by extracellular polymers [38]. For a gas-filled reservoir which is residually saturated with water, active microorganisms present in the water rely on the gas phase as a carbon and energy source, which means that they would grow mostly at the gas–water interface. This is supported by numerous studies in the fields of bioremediation, transport in the vadose zone, and microbially enhanced oil recovery in which bacterial cells have been observed to grow at the oil– or air–water interface [39–41]. Since the water phase is assumed to be immobile, the interface between the fluids (and hence the biofilm as well) can remain stable for extended periods.

As summarised in Fig. 2, three types of microorganisms are considered to be active in the presence of high concentrations of H_2:

$$\text{Methanogens}: 4H_2 + CO_2 \overset{\text{methanogens}}{\rightarrow} CH_4 + 2H_2O, \tag{1}$$

$$\text{Acetogens}: 4H_2 + 2CO_2 \overset{\text{acetogens}}{\rightarrow} CH_3COOH + 2H_2O, \tag{2}$$

$$\text{Acetotrophs}: CH_3COO^- + H^+ \overset{\text{acetotrophs}}{\rightarrow} CH_4 + CO_2. \tag{3}$$

Here, the term "methanogens" is used to refer to hydrogenotrophic methanogens (Archaea) which make use of CO_2 as the electron acceptor. The compounds in the above equations refer to aqueous species. Though dissolved CO_2 may exist as molecularly dissolved CO_2, carbonic acid, hydrogen carbonate, experimental data suggests that methanogenic reaction rates depend on undissociated CO_2 [42]. The concentration of dissociated CO_2 and the equilibrium between acetic acid and acetate depend on pH. In moderate to high concentrations, the dissociation reactions of the above-mentioned ions can themselves affect pH. However, for the conditions studied in this work, H_2 is the dominant gaseous species, and as such, only low concentrations of CO_2 (which is in equilibrium with gaseous CO_2) are achieved. Similarly, the presence of acetotrophs ensures a low concentration of acetic acid. Hence, the effect of these ions on pH is neglected. In addition,

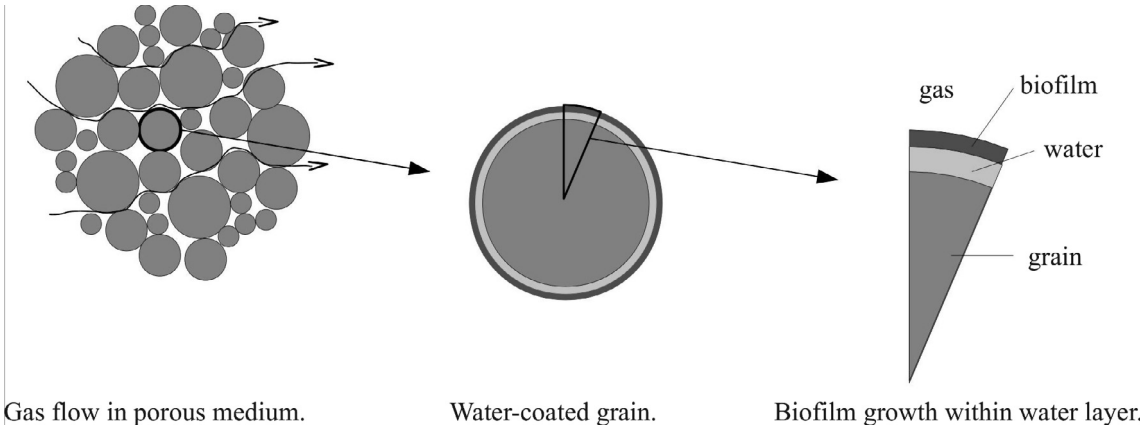

Fig. 1. Illustration of processes and assumptions: Gas flow through a porous medium in which the grains are coated with a thin water film in which microbes may grow.

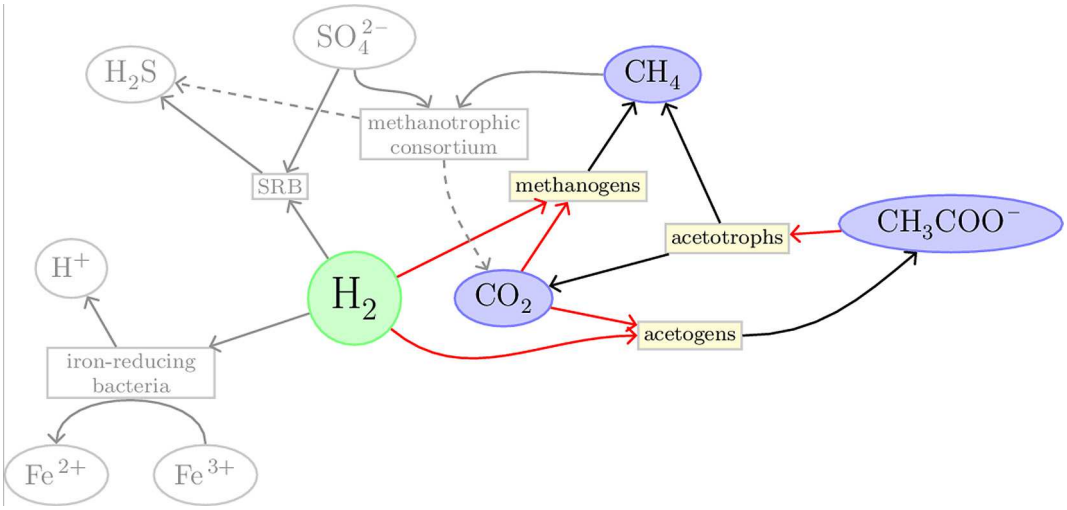

Fig. 2. Schematic representation of subsurface methanogenic microbial activity. The availability of sulphates and iron are assumed to be limited here. Hence, the organisms and reactions shown in grey are not accounted for in this work (see assumption in Section 2). SRB stands for sulphate-reducing bacteria. (For interpretation of the references to colour in this figure legend, the reader is referred to the web version of this article.)

the potential reduction in concentration of a given species (CO_2 or acetate) due to dissociation is neglected. As such, four aqueous species are accounted for by the model: dissolved H_2 and CH_4, undissociated CO_2, and acetate.

It is worth noting that some microorganisms are capable of reversing the methanogenic reaction in Eq. (1). However, this anaerobic methanotrophy can only be sustained if the H_2 produced is utilised immediately by other microbes, particularly, sulphate-reducing bacteria [43–45].

2.1.2. Biofilm growth

For the purposes of this work, a continuum model has been chosen. In this regard, a continuum is composed of microbial cells, extracellular polymers, and "void" (water-filled) spaces. Specifically, the mathematical model is based on the one proposed by Dockery and Klapper [18] and extended by Alpkvist and Klapper [46] for multi-species biofilms.

As stated in [18], the biofilm is treated as a homogeneous, viscous, and incompressible fluid of pressure p. Basically, biofilm growth is considered to be governed by an advective process, equivalent to the displacement of a mobile fluid (here the bulk fluid) by a less mobile one. Under the assumption that the biofilm is incompressible and density variations can be neglected (this means that microbial activity is assumed to be uniformly distributed within the biofilm), the following mass balance equation can be derived:

$$\nabla \cdot \mathbf{u} = \frac{q_f}{\varrho_f}. \tag{4}$$

Growth and decay in the biofilm are accounted for with the source/sink term q_f, directly related to the rate of change of biological volume. Note that ϱ_f is defined as the dry biofilm density. In this approach, the velocity $\mathbf{u}$ is assumed to be proportional to the gradient in pressure p. Growth or decay of biomass, indeed, can lead to a pressure build-up or reduction in the biofilm, resulting in biomass movement. In order to differentiate between p and the actual pressure of the bulk fluid, p will be referred to as a "biofilm pseudo-pressure". Hence,

$$\mathbf{u} = -\lambda \nabla p. \tag{5}$$

Here, λ is a constant that can be interpreted as the mobility of the biofilm. Eq. (5) is probably a rough representation of the momentum balance equation for the biofilm. However, the main process under consideration is free dilatation of the biofilm phase due to metabolic growth. No other mechanical constraint, e.g. as a result of the interaction with the viscous gas phase, is taken into account. This free dilatation model is well suited for the spherical one-dimensional geometry considered here.

In order to be able to track the interface between the biofilm and bulk water, the biofilm volume fraction ϕ_f is defined as

$$\phi_f = \frac{V_f}{V}, \tag{6}$$

where V_f is the volume occupied by the biofilm, and V is the total volume of a given representative elementary volume. Note that

$$0 \leqslant \phi_f \leqslant 1. \tag{7}$$

Then, even though Eq. (4) is solved in the whole domain to get $\mathbf{u}$, the velocity of the biofilm, $\mathbf{u}_f$ must be zero outside the biofilm. Thus,

$$\mathbf{u}_f = H_1(\phi_f)\,\mathbf{u}, \tag{8}$$

where H_1 is the Heaviside step function defined as:

$$H_1(\phi_f) = H(\phi_f - 1) = \begin{cases} 0, & \text{for } \phi_f < 1, \\ 1, & \text{for } \phi_f = 1. \end{cases} \tag{9}$$

It is approximated here as

$$H_1(\phi_f) \approx \phi_f^k \text{ (only valid for } 0 \leqslant \phi_f \leqslant 1), \tag{10}$$

which is exact for $k \to \infty$.

Now, a mass balance equation for the biofilm can be written as:

$$\frac{\partial \phi_f}{\partial t} + \nabla \cdot (\phi_f \mathbf{u}_f) = \frac{q_f}{\varrho_f}. \tag{11}$$

When $\phi_f = 1$, Eq. (11) reduces to Eq. (4). When $\phi_f < 1$, one obtains an ordinary differential equation with the first and last terms of Eq. (11).

Finally, inserting Eqs. (5) and (8), one obtains the following equation, expressed in spherical coordinates:

$$\frac{\partial \phi_f}{\partial t} - \frac{\lambda}{r^2}\frac{\partial}{\partial r}\left(H_1(\phi_f) r^2 \phi_f \frac{\partial p}{\partial r}\right) = \frac{q_f}{\varrho_f}. \tag{12}$$

This leads to a system of two equations, (4) and (12), and two unknowns, p and ϕ_f. To illustrate how these variables interact, a simple, one-dimensional simulation – obtained by solving Eqs. (4) and (12) using a finite-volume scheme – is shown in Fig. 3.

The biofilm itself is composed of the three microbial species, methanogens (m), acetogens (a), and acetotrophs (t), such that

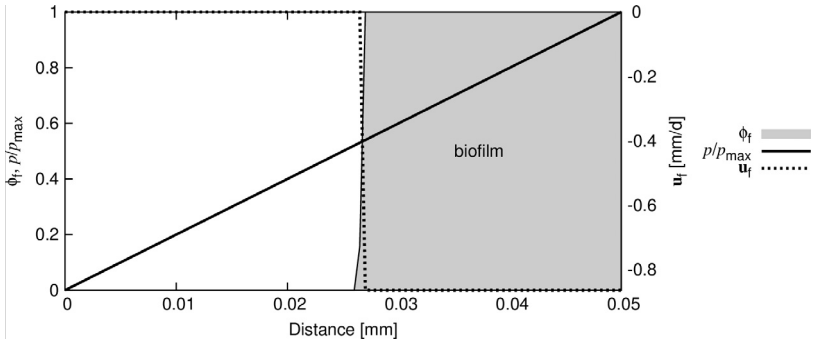

Fig. 3. Sample one-dimensional simulation of the growth of a biofilm (for $k = 100$ and $t = 27$ days). Initial conditions are $\phi_f = 10^{-5}$ and $p = 0$. The dashed line shows the velocity of the biofilm due to growth as a result of the gradient in p (continuous line). In this example, $\lambda = 8.64 \times 10^{-8}$ mm^2/d and the resulting $p_{max} = 500$. At the right boundary, $q_f/\varrho_f = 1.728$ d^{-1}, while, at the left boundary, there is no biomass flow and $p = 0$. This leads to biomass growth at the right and a displacement of the rest of the biofilm towards the left.

$$\phi_f = \phi_{f,m} + \phi_{f,a} + \phi_{f,t}. \tag{13}$$

Hence, the biofilm mass balance equation in Eq. (12) can be divided into:

$$\frac{\partial \phi_{f,i}}{\partial t} - \frac{\lambda}{r^2}\frac{\partial}{\partial r}\left(H_1(\phi_f) r^2 \phi_{f,i}\frac{\partial p}{\partial r}\right) = \frac{q_{f,i}}{\varrho_f}, \quad i \in \{m, a, t\}. \tag{14}$$

For the sake of completeness, Eq. (4) is also expressed in spherical coordinates:

$$-\frac{\lambda}{r^2}\frac{\partial}{\partial r}\left(r^2\frac{\partial p}{\partial r}\right) = \frac{q_f}{\varrho_f}. \tag{15}$$

Hence, Eqs. (13)–(15) determine the development of the biofilm within the water film.

2.1.3. Solute transport

The molar concentrations of four dissolved components – hydrogen, methane, carbon dioxide, and acetate – are considered, i.e. C_w^h, C_w^m, C_w^c, and C_w^a, respectively. For the transport of solutes, no explicit differentiation is made between the water and the biofilm phases (local mass equilibrium assumption). Hence, the above concentrations are both in water and in the biofilm. Assuming small Péclet numbers (see assumption on immobility of the water film in Section 2),

$$\frac{\partial C_w^i}{\partial t} - \frac{1}{r^2}\frac{\partial}{\partial r}\left(r^2 D_w^i \frac{\partial C_w^i}{\partial r}\right) = q_w^i, \quad i \in \{h, m, c, a\}. \tag{16}$$

The effective diffusion coefficient is assumed to be a linear function of ϕ_f, i.e.:

$$D_w^i = \phi_f D_{w,f}^i + (1 - \phi_f) D_{w,0}^i, \tag{17}$$

where $D_{w,0}^i$ is the aqueous diffusion coefficient in the absence of biofilms and $D_{w,f}^i$ is the effective diffusion coefficient in the biofilm. This is a simple way of accounting for the differences in diffusivity between the biofilm and the water phases.

At the boundary to the gas phase Γ_{wg}, i.e. the gas–water interface, Dirichlet boundary conditions for Eq. (16) are prescribed which depend on the gas-phase composition. This is done to account for the influence of the gas-phase composition on the concentrations of the dissolved components.

$$C_{w,\Gamma_{wg}}^i = K^i(p_g, T) \cdot \bar{x}_{g,\Gamma_{wg}}^i \quad i \in \{h, m, c\}, \tag{18}$$

where $K^i(p_g, T)$ is a solubility coefficient at the given pressure and temperature, and $C_{w,\Gamma_{wg}}^i$ is the value of C_w^i at the boundary Γ_{wg}. At this point, the average mole fraction of the gas-phase component at the interface, $\bar{x}_{g,\Gamma_{wg}}^i$, is assumed to be known (this will be discussed in Section 2.3).

Note that water and acetate are assumed not to partition into the gas phase. The saturated vapour pressures of water and acetic acid at 35 °C are 0.056 and 0.036 bar, respectively (data from the NIST database [47]), which, at a pressure of 100 bar, would result in gas-phase mole fractions of 0.56 and 0.36mmol/mol, respectively. As a result, these two components of the gas phase are neglected here. Hence, a no-flow condition is used for acetate at this boundary.

2.1.4. Sources and sinks

Sources and sinks in the balance Eqs. (14) and (16) are due to the growth and decay of biomass. In Eq. (14), it is given by:

$$q_{f,i} = r_{g,i} - r_{d,i}, \quad i \in \{m, a, t\}, \tag{19}$$

where $r_{g,i}$ are the microbial growth rates, and $r_{d,i}$ refers to the endogenous decay rate of the species i, calculated as a function of the constant decay coefficient b_0:

$$r_{d,i} = b_0 \varrho_f \phi_{f,i}, \quad i \in \{m, a, t\}. \tag{20}$$

In the following, the calculation of the various growth rates $r_{g,i}$ is described. However, it is important to note that if the considered domain (given volume of water) is completely filled with biofilm, no further growth of biofilm is possible. Once this happens, the value of $r_{g,i}$ tends to the rate of biofilm maintenance and is prevented from exceeding that of $r_{d,i}$, hence, avoiding biofilm growth outside the boundaries of the domain. Physically, this threshold value corresponds to the minimum consumption of nutrients required for maintenance purposes (endogenous metabolism).

Growth rate of methanogens. In general, it is assumed that Monod kinetics (e.g. [48]) can sufficiently reproduce the rates at which these subsurface microbial processes occur. Hence, the growth rate of the hydrogenotrophic methanogens can be expressed as (cf. Eq. (1)):

$$r_{g,m} = \mu_m \varrho_f \phi_{f,m}\left(\frac{C_w^h}{C_w^h + K_{hm}}\right)\left(\frac{C_w^c}{C_w^c + K_{cm}}\right), \tag{21}$$

where μ_m is the maximum growth rate of the methanogenic microorganisms, and K_{hm} and K_{cm} are the half-saturation constants of H_2 and CO_2, respectively.

Several studies have dealt with the quantification of μ_m and K_{hm} which may vary with specific microbial species:

μ_m	0.3–4.1d^{-1}	[49],
K_{hm}	4.2 μM	[50],
	5 μM	[42],
	4–16 μM	[51],
	5.8–7.3 μm	[49].

However, with some interesting exceptions (e.g., [52]), the availability of CO_2 is rarely considered to be a limiting factor, and hence, there is little information on the value of K_{cm}. Dornseiffer et al. [42] suggest, based on experimental data, that the molar concentration used in Eq. (21) for CO_2 should be that of undissociated CO_2. The corresponding value of K_{cm} observed by Dornseiffer et al. [42] is 0.23 mM and as such several orders of magnitude higher than K_{hm}.

Growth rate of acetogens. Based on Eq. (2), the following growth rate for hydrogenotrophic acetogens can be assumed:

$$r_{g,a} = \mu_a \varrho_f \phi_{f,a} \left(\frac{C_w^h}{C_w^h + K_{ha}} \right) \left(\frac{C_w^c}{C_w^c + K_{ca}} \right), \tag{22}$$

where μ_a is the maximum growth rate of the acetogenic microorganisms, and K_{ha} and K_{ca} are the half-saturation constants of H_2 and CO_2, respectively. Literature values for these parameters include:

μ_a[1]	0.4–1.9d^{-1}	[53],
K_{ha}	1.3–3.7 μM	[54].

The values given above for K_{ha} are similar in range to those of K_{hm}. It will be assumed here that K_{ca} is also in the same range as K_{cm}.

Growth rate of acetotrophs Literature on methanogenic acetotrophs is readily available. The growth rate of these microorganisms (cf. Eq. (3)) can be estimated as:

$$r_{g,t} = \mu_t \varrho_f \phi_{f,t} \frac{C_w^a}{C_w^a + K_t}, \tag{23}$$

where μ_t is the maximum growth rate of acetotrophic microorganisms, and K_t is the half-saturation constant of acetate.

Good sources for the parameters of Eq. (23) are given below along with the parameter values.

μ_t	0.08 – 0.69d^{-1}	[55],
K_t	0.46 mM	[56],
	0.4–3 mM	[49, 55],

Consumption/production of dissolved components. Based on the microbial reactions, the consumption and production of the various dissolved components required in Eq. (16) read:

$$q_w^h = -\frac{r_{g,m}}{Y_m} - \frac{r_{g,a}}{Y_a}, \tag{24}$$

$$q_w^m = \frac{r_{g,m}}{4Y_m} + \frac{r_{g,t}}{Y_t}, \tag{25}$$

$$q_w^c = -\frac{r_{g,m}}{4Y_m} - \frac{r_{g,a}}{2Y_a} + \frac{r_{g,t}}{Y_t}, \tag{26}$$

$$q_w^a = \frac{r_{g,a}}{4Y_a} - \frac{r_{g,t}}{Y_t}. \tag{27}$$

The coefficients of the rates above account for the stoichiometry of the reactions. Here, Y_i refers to yield coefficients (dry biomass per mole of substrate) which have values in the following ranges.

Y_m	0.3–2.2 g/mol H_2	[49],
	0.62 g/mol H_2	[57],
Y_a	0.35–0.85 g/mol H_2	[53],
	2.75 g/mol H_2	[57],
Y_t	2.52 g/mol A_c	[57].

[1] For mesophilic homoacetogens growing on H_2/CO_2.

2.2. Gas flow and transport

As stated in Section 2, at a sufficiently large distance from the injection point, the advective flow in the gas phase can be assumed to be relatively slow. This allows the use of Stokes' equations to describe gas flow in this domain:

$$\mu_g \nabla \cdot \nabla \mathbf{u}_g + \mathbf{f} = \nabla p_g; \tag{28}$$

$$\nabla \cdot \mathbf{u}_g = 0. \tag{29}$$

Here, μ_g is the viscosity, $\mathbf{u}_g$ the gas velocity, and p_g the pressure of the gas phase, while $\mathbf{f}$ accounts for external body forces. As can be seen above, the flow is assumed to be stationary, and compressibility and density-variation effects are neglected. Due to the large difference between the time scales of advection and biofilm activity (see Section 1.2), gas flow and transport can be assumed to be quasi-steady on the advective time scale, i.e. changes in gas-phase composition (and the corresponding changes in density) do not occur at this scale. In addition, the dependence of the gas-phase density on pressure is negligible due to low variations in pressure at the length scale under consideration (several millimetres).

The interface Γ_{wg} is a no-flow boundary, i.e.:

$$\mathbf{u}_g \cdot \mathbf{n} = 0, \quad \text{at } \Gamma_{wg}. \tag{30}$$

Mass exchange at the interface being small, we assume that the transport of the various components of the gas phase can be accounted for with the following transport equations:

$$\nabla \cdot (\mathbf{u}_g c_g x_g^i) - \nabla \cdot (c_g D_g^i \nabla x_g^i) = 0, \quad i \in \{h, c\}, \tag{31}$$

where c_g is the total molar concentration of the gas phase. Additionally,

$$\sum_i x_g^i = 1, \quad i \in \{h, m, c\}. \tag{32}$$

In this multicomponent transport model, the following assumptions have been made:

- The diffusion matrix coming from the Maxwell–Stefan theory is approximated by its diagonal value, the diagonal terms themselves being estimated from binary diffusion terms.
- The component equations are written on a molar basis, and we use the assumption that the molar average velocity is approximately equal to the mass average velocity, $\mathbf{u}_g$, used in the Stokes equation, hence the use of $\mathbf{u}_g$ in Eq. (31) (cf. [58]).

As stated in Section 2.1.3, acetate is not considered to be present in the gas phase. The molar flux of each component across the gas–water interface Γ_{wg} is accounted for with the boundary conditions:

$$-\left(c_g D_g^i \nabla x_g^i\right)\Big|_{\Gamma_{wg}} \cdot \mathbf{n} = -(D_w^i \nabla C_w^i)\Big|_{\Gamma_{wg}} \cdot \mathbf{n}, \quad i \in \{h, m, c\}. \tag{33}$$

Obviously, the right-hand side of Eq. (33) can only be calculated if the gradient of the concentration of the component i in the water/biofilm phase (i.e. ∇C_w^i) is available.

2.3. Coupled model

The coupling of the models for biofilm growth in the water film around the grains (Section 2.1) and for the gas flow through the porous medium (Section 2.2) is described in this section, while keeping the respective temporal and spatial scales of the individual models. Let Ω_g be the gas-phase domain, Ω_w the water-film domain (which may contain water and biofilm), and Γ_{wg} the interface between the two. The basic coupling principle can be summarised

based on these definitions and the assumption of spherically symmetric grains as follows:

1. Solve the flow equations in Ω_g with Eqs. (28)–(30).
2. Solve the transport equations for the components of the gas phase in Ω_g with Eqs. (31)–(33).
3. Calculate an average mole fraction $\bar{x}^i_{g,\Gamma_{wg}}$ for each component of the gas phase at the gas–water interface Γ_{wg} for each grain, i.e.

$$\bar{x}^i_{g,\Gamma_{wg}} = \frac{\int x^i_g \mathrm{d}\Gamma_{wg}}{\int \mathrm{d}\Gamma_{wg}}. \tag{34}$$

4. Assuming spherical symmetry of each grain, calculate the dissolved molar concentration $C^i_{w,\Gamma_{wg}}$ of each component at the gas–water interface as a function of $\bar{x}^i_{g,\Gamma_{wg}}$ using the gas solubility as in Eq. (18).
5. Use $C^i_{w,\Gamma_{wg}}$ as boundary conditions to solve for biofilm growth and component diffusion in the water film (Ω_w) of each grain (Eqs. (13)–(16)) in spherical coordinates with rotational symmetry.
6. Using the new distribution of C^i_w for each grain, update the boundary conditions of the gas transport equations as in Eq. (33).
7. Repeat Steps 2–6 till convergence is reached.

2.4. Numerical discretisation

For the biofilm and solute transport model, the partial differential equations are discretised in space with a vertex-centred finite-volume method and in time with an implicit Euler scheme. This is implemented within the flow simulator MUFTE-UG [59].

The Stokes flow equations are discretised with a finite-volume method, using the Uzawa scheme [26]. The transport equations are also discretised with a finite-volume method with an upwinding scheme (for more detail, see [26]).

Finally, the two models are coupled iteratively using the Picard method. The values of $\bar{x}^i_{g,\Gamma_{wg}}$ and $(D^i_w \nabla C^i_w)\big|_{\Gamma_{wg}} \cdot \mathbf{n}$ are monitored for convergence.

3. Example of model application

In order to show the capabilities of the coupled model described in Section 2.3, a model simulation is presented here as an example. A model domain of dimension 6.83 mm × 1.83 mm × 1.83 mm consisting of 34 spherical grains is considered. The domain contains uniformly packed grains of radius $r_g = 0.41$ mm as shown in Fig. 4. Note that the geometry is not supposed to be representative of a realistic reservoir rock. At this point, a simplified porous system (packed bed of uniform grains) is sufficient to investigate the physical processes involved and the coupling between biofilm growth and hydrogen consumption.

In the following, the description of the simulation is divided into two parts, one for each sub-model.

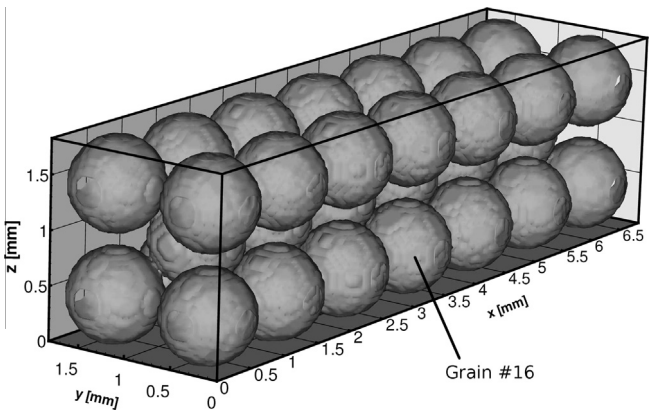

Fig. 4. Simulation domain showing the arrangement of 34 spherical grains. The marked grain is studied in Section 3.3.

3.1. Gas flow and transport

It is assumed that there is a constant flow of a gas mixture through the domain. The domain is discretised with 165 × 55 × 55 finite volumes. The gas is composed of (in molar fractions) 95% H_2, 4.96% CH_4, and 0.04% CO_2. Hence, the availability of CO_2 may limit microbial activity. Realistic storage conditions [5] of 100 bar and 35 °C are assumed to prevail. At these conditions, the total molar concentration and viscosity of the gas are estimated to be 3780 mol/m^3 and 10 μPa s.

The maximum solubilities of CH_4 [60] and CO_2 [61] in water at the given conditions are 0.089 mol/l and 1.27 mol/l, respectively. As for H_2, its maximum solubility is calculated from its Henry constant at 100 bar (e.g. [62]) as 0.071 mol/l. Note that the maximum solubilities are multiplied by their respective gas-phase mole fractions to obtain the actual concentrations in water (see Eq. (18)).

The diffusion coefficients of the components of the gas phase are calculated as proposed by Fairbanks and Wilke [63]. The binary gas diffusion coefficients, which are needed for the calculation, are computed using the correlations given by Fuller et al. [64]. For the given gas composition and physical conditions, these result in the following diffusion coefficients:

$$D^h_g = 7.26 \times 10^{-7}\ \mathrm{m}^2/\mathrm{s},$$
$$D^c_g = 5.98 \times 10^{-7}\ \mathrm{m}^2/\mathrm{s}.$$

Boundary conditions. Periodic boundary conditions are used for the Stokes flow equations, and an average pressure gradient, e.g., as a result of the injection pressure at the borehole, is maintained in the domain, i.e.

$$\nabla p_g - \mathbf{f} = \begin{pmatrix} -0.001 \\ 0 \\ 0 \end{pmatrix} \mathrm{Pa/m}. \tag{35}$$

Here $\mathbf{f}$ represents gravitational forces.

At the inflow boundary ($x = 0$ mm, see Fig. 4), the mole fractions of the various gases are constant and as given previously, i.e. 95% H_2, 4.96% CH_4, and 0.04% CO_2. At the outflow boundary ($x = 6.83$ mm), the diffusive fluxes in x-direction are set to zero (Danckwerts conditions). All other boundaries are no-flow boundaries.

3.2. Biofilm growth

The thickness l_w of the water films that coat the grains is assumed to be proportional to the size of the grains and discretised spatially with 25 nodes. Assuming a residual water saturation of 0.2, this yields $l_w = 0.08 r_g$ for each grain. As stated previously, this is only possible under the assumption that the water is uniformly distributed in the medium and coats the grains as films. This neglects possible water accumulation at grain contact points, i.e. pendular rings.

Initially, all concentrations and the biofilm pseudo-pressure are zero, and the volume fraction of each of the three microbial species considered is assigned a small value (10^{-5}). The boundary conditions at the gas–water interface are as stated in Section 2.2. In addition:

- There is no flow of biomass across the gas–water interface.

At the grain–water boundary, the following conditions are applied:

- The biofilm pseudo-pressure is set to zero.
- There is no flow of biomass, dissolved gases, or acetate across this boundary.
- The consumption rate of all microbial species are reduced to the needs of endogenous metabolism once the biofilm completely fills the water film.

Table 1
Growth and decay parameters used in simulation.

Parameter	Value
Maximum growth rate (1/d)	
μ_m	0.65
μ_a	0.40
μ_t	0.50
Yield coefficients	
(g/mol H_2)	
Y_m	0.5
Y_a	0.5
(g/mol A_c)	
Y_t	2.5
Half-saturation coefficients	
H_2 (μ mol/l)	
K_{hm}	5
K_{ha}	5
CO_2 (m mol/l)	
K_{cm}	0.3
K_{ca}	0.1
Acetate (m mol/l)	
K_t	1
Endogenous decay constant (1/d)	
b_0	0.06

As suggested by Stewart [65], the diffusion in the biofilm is estimated with:

$$D^i_{w,f} = 0.6 D^i_{w,0} \tag{36}$$

for light gases (in this case, this value is used for H_2, CH_4, and CO_2), and

$$D^i_{w,f} = 0.25 D^i_{w,0} \tag{37}$$

for organic solutes (in this case, acetate). The values given in [65] for $D^i_{w,0}$ are used here:

$$D^h_w = 4.50 \times 10^{-9}\ \mathrm{m^2/s},$$
$$D^m_w = 1.49 \times 10^{-9}\mathrm{m^2/s},$$
$$D^c_w = 1.92 \times 10^{-9}\mathrm{m^2/s},$$
$$D^a_w = 1.29 \times 10^{-9}\mathrm{m^2/s}.$$

The biofilm density ϱ_f is 100 g/l, which, compared to the values in [66], represents a dense biofilm. The parameter k is chosen to be 100. The parameters for the growth kinetics of all three microbial species are given in Table 1. These parameters have been chosen to lie within the ranges of values given in Section 2.1.2. For this particular case, the methanogens have a higher maximum growth rate than the acetogens, and hence will be more dominant.

3.3. Results

The distribution of the magnitude of velocity in the domain is shown for a slice through the z-plane in Fig. 5. Flow is from left to right. Reynolds numbers do not exceed 1.5×10^{-4}. For the same slice, the distribution of the CO_2 mole fraction in the gas phase is shown in Fig. 6. During peak microbial activity, the largest varia-

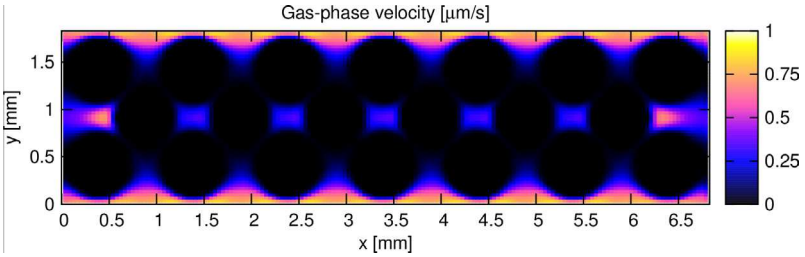

Fig. 5. A slice through the z-plane at $z = 0.7$ mm showing the magnitude of the gas-phase velocity $||\mathbf{u}_g||$. This does not vary with time and is solved for only once.

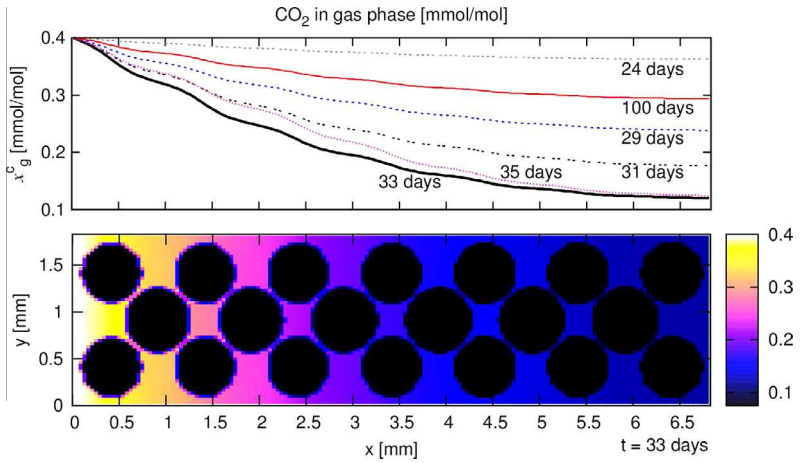

Fig. 6. The plot at the top shows the mole fraction of CO_2, x^c_g, along the x-axis for $y = z = 0$ mm at different points in time, while the bottom figure shows x^c_g, on a slice through the z-plane at $z = 0.7$ mm and $t = 33$ days.

tion of the CO_2 concentration around a grain from its average grain value was approximately 5%. In this simulation, the availability of CO_2 limits growth. It can be seen that a significant amount of CO_2 is consumed as it passes through the domain. The rate at which this occurs depends on the concentration of CO_2 as the growth-limiting component and the state of development of the biofilm in each water film in the different parts of the domain. As the biofilms grow, the consumption rate increases. However, when a water film is filled with biofilm, the biofilm only consumes the amount required for maintenance. This is the case, for instance, for the curve at $t = 100$ days, which shows a lower consumption than at earlier times. In addition, the lower CO_2 concentration towards the right boundary leads to a reduced consumption (and growth) rate. This can be seen in the gradient most of the curves in Fig. 6, which tend to decline towards the right.

For one of the grains in the domain (see grain marked in Fig. 4), the biofilm volume fraction and the concentration of CO_2 within the water film that coats the grain are shown in Fig. 7 for $t = 33$ days. The biofilm has filled the area near the gas–water interface, and is growing towards the grain–water interface. The availability of CO_2 declines towards the grain–water interface, hence the uneven growth of the biofilm. Figs. 8 and 9 show the development of the biofilm and the corresponding CO_2 concentration in water over time. At early times, biofilm growth is completely uniform since there is no shortage of CO_2 in the domain. This changes as the amount of active biomass increases leading to growth limitation near the grain–water interface.

The biofilm is composed of the three species (methanogens, acetogens, and acetotrophs) as shown in Fig. 10. Since there is an excess of H_2, the methanogens compete with the acetogens for CO_2, while the acetotrophs produce CO_2. Due to the higher specific growth rate of the methanogens (as used in this simulation), the methanogens dominate the biofilm, while the acetogens and acetotrophs together make up less than 20% of the biofilm. Due to the diversity of microorganisms, this may not be the case in general. However, literature values for the kinetic growth parameters of methanogens and acetogens (see Section 2.1.2) suggest higher methanogenic growth rates. The illustrative snapshot of the spatial variations of the biofilm population in Fig. 10 after 33 days shows that, even though methanogenic activity prevails globally, it is slightly less dominant towards the grain–water interface due to the reduced CO_2 concentration (see Fig. 7). In this example, the acetogenic half-saturation constant for CO_2 is lower than that of the methanogens, giving the acetogenic/acetotrophic consortium

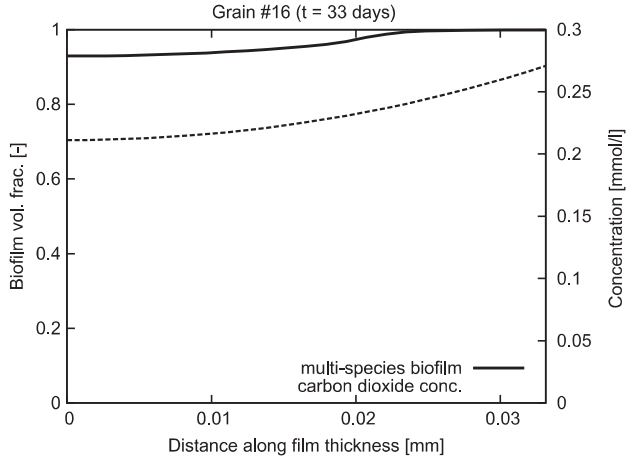

Fig. 7. Microbial growth in the water film which coats one of the grains. The biofilm completely occupies the space near the gas–water interface (at 0.033 mm), while still growing further towards the grain–water interface (at 0 mm). The concentration of CO_2, which is growth limiting, within the water/biofilm is also shown.

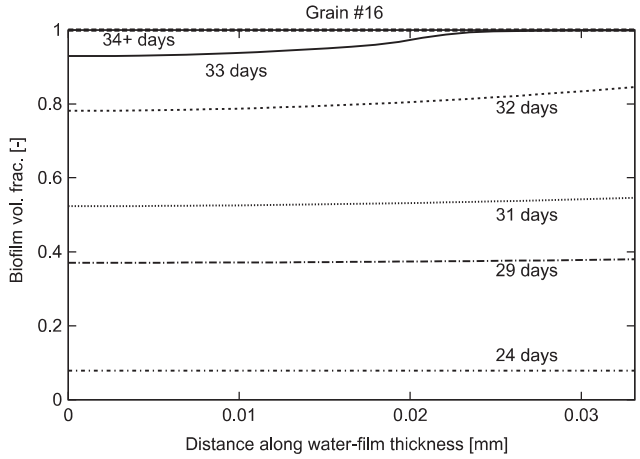

Fig. 8. Temporal evolution of microbial growth in the water film which coats one of the grains. The grain–water interface is at 0 mm, while the gas–water interface is at 0.033 mm.

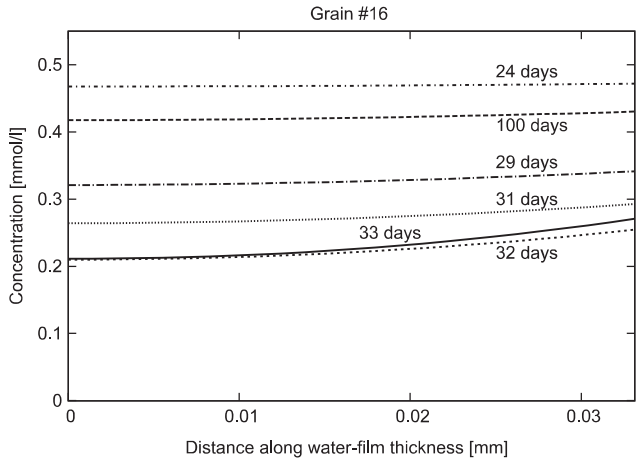

Fig. 9. Temporal evolution of CO_2 concentration in the water film which coats one of the grains. The grain–water interface is at 0 mm, while the gas–water interface is at 0.033 mm.

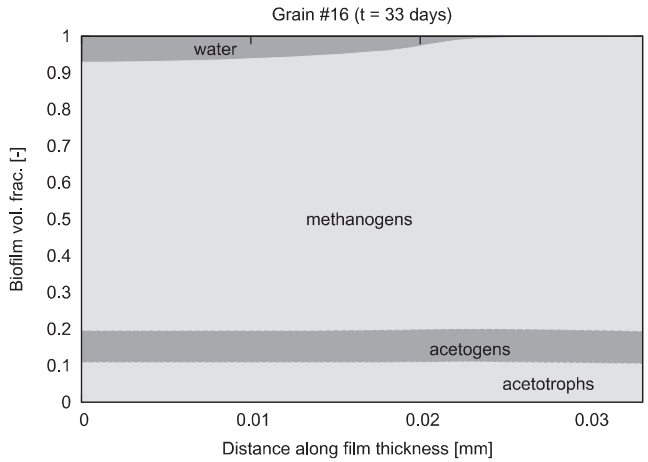

Fig. 10. Distribution of microbial species within the water film around one of the grains. The grain–water interface is at 0 mm, while the gas–water interface is at 0.033 mm. The methanogens dominate the acetogens and acetotrophs.

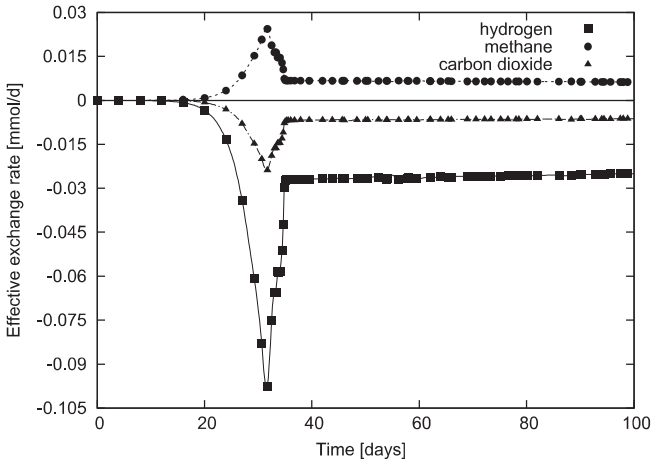

Fig. 11. Effective exchange rates between the gas phase and the biofilm/water phase for the whole domain over time.

a small advantage in regions of low CO_2 concentration within the biofilm.

To give a first example of the effective macroscopic parameters which can be extracted from such pore-scale simulations and, ultimately, implemented in reservoir-scale models, the effective rates of microbial H_2 and CO_2 consumption and CH_4 production have been calculated. As the gas passes through the domain, the rates change with time depending on the amount and activity of biomass in the domain. As shown in Fig. 11, the total/effective exchange rates between the biofilm/water and gas phases increase strongly at $t \approx 20$ days. This is due to the fast growth of biomass. At some point, some of the water films become filled with biofilm, leading to a slowdown of the exchange rates. At $t \approx 35$ days, all the water films are saturated with biofilms. At this point, the consumption of the gases is reduced to the amount required for maintenance. This leads to constant conversion rates, suggesting the possibility of using a simplified model at late times.

3.4. Model sensitivity: impact of initial water saturation

In order to study the influence of the amount of water in the porous medium on the behaviour of the system and, in particular, on the temporal evolution of the conversion rates, two further simulations are presented in this section which are identical to that of Sections 3.1–3.3 except that the thickness l_w of the water films that coat the grains are varied as follows:

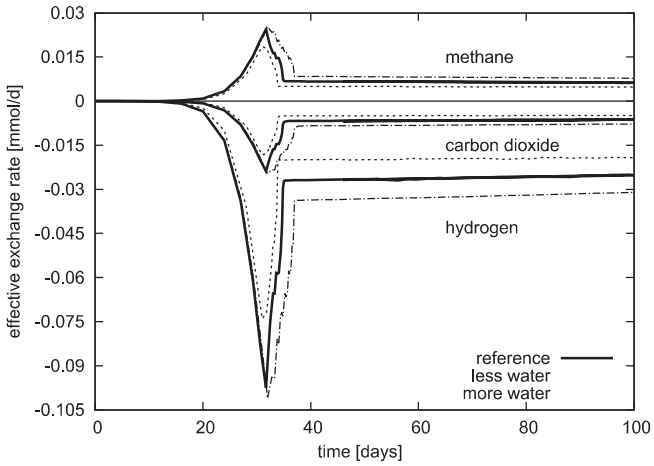

Fig. 12. Comparison of effective exchange rates between the gas phase and the biofilm/water phase for the whole domain over time.

(a) Water saturation $S_w = 0.15$ (i.e., $l_w = 0.06 \cdot R_g$),;
(b) Water saturation $S_w = 0.25$ (i.e., $l_w = 0.10 \cdot R_g$),.

The resulting conversion rates of the dissolved gases (see Fig. 12) show that:

- Thicker water films allow, as expected, longer periods of active microbial growth due to the larger amount of space available than thinner films.
- The peak conversion rate is higher the thicker the water film since it takes a longer period of time for each individual water film to fill up with biomass.
- The steady-state conversion rate is also higher the thicker the water film. This is due to the fact that thicker biofilms require more substrate for maintenance.

4. Summary and conclusions

From the results described in this work, our primary conclusions and comments for future research on this problem are as follows:

- Microorganisms capable of making use of H_2 as an energy source may have a significant impact on the efficiency of underground hydrogen storage operations.
- A numerical model is presented which couples biofilm-scale processes to pore-scale flow and transport processes. The algorithm models the biofilm-scale processes in uniform films of residual water which are assumed to coat the grains of the porous medium and couples these to gas flow through the pores. The model does not account for a heterogeneous water distribution within the porous medium. To an extent, this restricts its applicability since an uneven water distribution may lead to a more heterogeneous biomass distribution.
- The biofilm model is based on a viscous-fluid model [18,46] and accounts for three microbial species (methanogens, acetogens, and acetotrophs) as well as the diffusion and consumption/production of dissolved components. On the pore scale, Stokes' flow equations are solved, and the transport of the gas components, H_2, CH_4, and CO_2, is simulated. These two models are coupled via boundary conditions (including an exchange flux term).
- Depending on the composition of the stored gas, methanogens and acetogens compete for H_2 and CO_2. Literature values for the kinetic growth parameters of these micro-organisms suggest higher methanogenic growth rates. Nonetheless, it is possible for both to coexist.
- The rate of conversion of H_2 and CO_2 to CH_4 depends on the amount and activity of biomass present. However, when the available residual water is saturated with biomass, the conversion rates approach a steady state, which is the amount the microbes require for maintenance.
- Variations in the thickness of the water films show that the steady-state conversion rates vary with the amount of residual water in the porous medium. Thicker water films lead to thicker biofilms which require more substrate.

5. Outlook

- The model concept needs to be extended to account for a more realistic geometry and water distribution in the porous medium, particularly at grain contact points.
- The dissociation of CO_2 in water and the effects of the mineral phase on the microbial processes are important issues that are not yet accounted for by this model.

- Future work should also consist of extending the biofilm model to account for a greater number of species which may compete with methanogens and acetogens for H_2. Sulphate-reducing bacteria, for example, may convert H_2 to hydrogen sulphide in the presence of sulphates which could have a very detrimental effect on a UHS operation.
- Experimental observations will be required in parallel to confront our numerical predictions. To this end, an experimental study in flow-through triaxial cells is currently being carried out. The effective kinetics of H_2 consumption under flow conditions will be characterised in the presence and in the absence of bacteria on cylindrical samples of reservoir rocks (limestone and sandstone) under the stress, pressure, and temperature conditions of underground storage.
- The effect of these biofilm- and pore-scale processes on the field scale certainly has to be investigated. Effective conversion rates can be extracted from simulations using this model and implemented in larger-scale models. This can be achieved, for example, by running several possible simulation configurations and numerically determining constitutive relationships.

Acknowledgement

This work was partially supported by the Region of Lorraine and by Carnot Funding (Grant Hydrogène, Institut Carnot ICEEL).

Appendix A. Notation

Symbol	Definition	Unit
C_w	molar concentration of component in water/biofilm	mol/l
D	diffusion coefficient	m^2/s
H	Heaviside step function	–
K	solubility coefficient	mol/l
R_g	grain radius	mm
S	saturation	
V	control volume	l
V_f	biofilm volume	l
Y	yield coefficient	g/mol H_2 or g/mol A_c
b_0	biomass decay coefficient	1/d
k	parameter for step function	–
c_g	total molar concentration of gas phase	mol/m^3
$\mathbf{f}$	external body forces	N/m^3
l_w	thickness of water film	mm
$\mathbf{n}$	unit normal vector	–
p	biofilm pseudo-pressure	–
p_g	gas-phase pressure	Pa
q_f	sources/sinks of biomass	g/(l d)
q_w	sources/sinks of components in water/biofilm	mol/(l d)
r_d	endogenous biomass decay rate	g/(l d)
r_g	biomass growth rate	g/(l d)
$\mathbf{u}$	Velocity of biomass displacement due to biofilm growth	dm/s
$\mathbf{u}_g$	gas-phase velocity	m/s
x_g	mole fraction	mol/mol
Γ_{wg}	gas–water interface	dm^2
Ω_g, Ω_w	gas and biofilm/water domains	l
ϕ_f	biofilm volume fraction	–
λ	mobility of biofilm	dm^2/s mm^2/d

Appendix A (*continued*)

Symbol	Definition	Unit
μ_m, μ_a, μ_t	maximum specific growth rate of microbial species	1/d
μ_g	gas-phase viscosity	Pa s
ϱ_f	dry biofilm density	g/l
Superscripts		
a	acetate	
c	carbon dioxide	
h	hydrogen	
m	methane	
Subscripts		
a	acetogens	
d	decay	
f	biofilm	
g	gas or growth	
m	methanogens	
t	acetotrophs	
w	water	

References

[1] Andrews J, Shabani B. Re-envisioning the role of hydrogen in a sustainable energy economy. Int J Hydrogen Energy 2012;37(2):1184–203. http://dx.doi.org/10.1016/j.ijhydene.2011.09.137.

[2] Simbeck DR. CO2 capture and storage—the essential bridge to the hydrogen economy. Energy 2004;29(9–10):1633–41. http://dx.doi.org/10.1016/j.energy.2004.03.065.

[3] Taylor J, Alderson J, Kalyanam K, Lyle A, Phillips L. Technical and economic assessment of methods for the storage of large quantities of hydrogen. Int J Hydrogen Energy 1986;11(1):5–22. http://dx.doi.org/10.1016/0360-3199(86)90104-7.

[4] Stone HBJ, Richardson RN, Veldhuis I. An investigation into large-scale hydrogen energy storage in the UK, At international hydrogen energy congress & exhibition, Istanbul, Turkey, 13–15, 2005.

[5] Panfilov M. Underground storage of hydrogen: in situ self-organisation and methane generation. Transp Porous Med 2010;85:841–65. http://dx.doi.org/10.1007/s11242-010-9595-7.

[6] Truche L, Jodin-Caumon M, Lerouge C, Berger G, Mosser-Ruck R, Giffaut E, Michau N. Sulphide mineral reactions in clay-rich rock induced by high hydrogen pressure. Application to disturbed or natural settings up to 250 °C and 30 bar. Chem Geol 2013;351:217–28. http://dx.doi.org/10.1016/j.chemgeo.2013.05.025.

[7] Lovley DR, Chapelle FH. Deep subsurface microbial processes. Rev Geophys 1995;33(3):365–81. http://dx.doi.org/10.1029/95RG01305.

[8] Kotelnikova S. Microbial production and oxidation of methane in deep subsurface. Earth Sci Rev 2002;58(3–4):367–95. http://dx.doi.org/10.1016/S0012-8252(01)00082-4.

[9] Šmigáň P, Greksák M, Kozánková J, Buzek F, Onderka V, Wolf I. Methanogenic bacteria as a key factor involved in changes of town gas stored in an underground reservoir. FEMS Microbiol Lett 1990;73(3):221–4. http://dx.doi.org/10.1111/j.1574-6968.1990.tb03944.x.

[10] Buzek F, Onderka V, Vančura P, Wolf I. Carbon isotope study of methane production in a town gas storage reservoir. Fuel 1994;73(5):747–52. http://dx.doi.org/10.1016/0016-2361(94)90019-1.

[11] Stone H, Veldhuis I, Richardson R. Underground gas storage: worldwide experiences and future development in the UK and Europe. Underground hydrogen storage in the UK, vol. 313. Geological Society, London, Special Publications; 2009 (pp. 215–24).

[12] Carden P, Paterson L. Physical, chemical and energy aspects of underground hydrogen storage. Int. J Hydrogen Energy 1979;4(6):559–69. http://dx.doi.org/10.1016/0360-3199(79)90083-1.

[13] Lindblom U. A conceptual design for compressed hydrogen storage in mined cavern. Int J Hydrogen Energy 1985;10(10):667–75. http://dx.doi.org/10.1016/0360-3199(85)90006-0.

[14] Paterson L. The implication of fingering in underground hydrogen storage. Int J Hydrogen Energy 1983;8(1):53–9. http://dx.doi.org/10.1016/0360-3199(83)90035-6.

[15] Ebigbo A, Helmig R, Cunningham A, Class H, Gerlach R. Modelling biofilm growth in the presence of carbon dioxide and water flow in the subsurface. Adv Water Resour 2013;33(10):667–75. http://dx.doi.org/10.1016/j.advwatres.2010.04.004.

[16] Wang Q, Zhang T. Review of mathematical models for biofilms. Solid State Commun 2010;150(21–22):1009–22. http://dx.doi.org/10.1016/j.ssc.2010.01.021.

[17] Wimpenny JWT, Colasanti R. A unifying hypothesis for the structure of microbial biofilms based on cellular automaton models. FEMS Microbiol Ecol 1997;22(1):1–16. http://dx.doi.org/10.1111/j.1574-6941.1997.tb00351.x.

[18] Dockery J, Klapper I. Finger formation in biofilm layers. SIAM J Appl Math 2002;62(3):853–69. http://dx.doi.org/10.1137/S0036139900371709.

[19] Kreft J-U, Picioreanu C, Wimpenny JWT, van Loosdrecht MCM. Individual-based modelling of biofilms. Microbiology 2001;147(11):2897–912.

[20] Picioreanu C, van Loosdrecht M, Heinen J. Mathematical modeling of biofilm structure with a hybrid differential-discrete cellular automaton approach. Biotechnol Bioeng 1998;58(1):101–16. http://dx.doi.org/10.1002/(SICI)1097-0290(19980405)58:1.

[21] Dupin H, Kitanidis P, McCarty PL. Pore-scale modeling of biological clogging due to aggregate expansion: a material mechanics approach. Water Resour Res 2001;37(12):2965–79. http://dx.doi.org/10.1029/2001WR000306.

[22] Knutson CE, Werth CJ, Valocchi AJ. Pore-scale simulation of biomass growth along the transverse mixing zone of a model two-dimensional porous medium. Water Resour Res 2005;41:W07007. http://dx.doi.org/10.1029/2004WR003459.

[23] Kapellos GE, Alexiou TS, Payatakes AC. Hierarchical simulator of biofilm growth and dynamics in granular porous materials. Adv Water Resour 2007;30(6–7):1648–67. http://dx.doi.org/10.1016/j.advwatres.2006.05.030.

[24] Pintelon T, Picioreanu C, van Loosdrecht M, Johns M. The effect of biofilm permeability on bio-clogging of porous media. Biotechnol Bioeng 2012;109(4):10031–1042. http://dx.doi.org/10.1002/bit.24381.

[25] Ginn TR, Wood BD, Nelson KE, Scheibe TD, Murphy EM, Clement TP. Processes in microbial transport in the natural subsurface. Adv Water Resour 2002;25(8–12):1017–42. http://dx.doi.org/10.1016/s0309-1708(02)00046-5.

[26] Golfier F, Wood BD, Orgogozo L, Quintard M, Buès M. Biofilms in porous media: development of macroscopic transport equations via volume averaging with closure for local mass equilibrium conditions. Adv Water Resour 2009;32:463–85. http://dx.doi.org/10.1016/j.advwatres.2008.11.012.

[27] Eberhard J, Efendiev Y, Ewing R, Cunningham A. Coupled cellular models for biofilm growth and hydrodynamic flow in a pipe. Int J Multiscale Comput 2005;3(4):499–516. http://dx.doi.org/10.1615/IntJMultCompEng.v3.i4.70.

[28] Wood BD, Radakovich K, Golfier F. Effective reaction at a fluid–solid interface: applications to biotransformation in porous media. Adv Water Resour 2007;30(6–7):1630–47. http://dx.doi.org/10.1016/j.advwatres.2006.05.032.

[29] Orgogozo L, Golfier F, Bues M, Quintard M. Upscaling of transport processes in porous media with biofilms in non-equilibrium conditions. Adv Water Resour 2010;33(5):585–600. http://dx.doi.org/10.1016/j.advwatres.2010.03.004.

[30] van Noorden TL, Pop IS, Ebigbo A, Helmig R. An upscaled model for biofilm growth in a thin strip. Water Resour Res 2010;46:W06505. http://dx.doi.org/10.1029/2009WR008217.

[31] Helmig R, Flemisch B, Wolff M, Ebigbo A, Class H. Model coupling for multiphase flow in porous media. Adv Water Resour 2013;51:52–66. http://dx.doi.org/10.1016/j.advwatres.2012.07.003.

[32] Scheibe TD, Tartakovsky AM, Tartakovsky DM, Redden GD, Meakin P. Hybrid numerical methods for multiscale simulations of subsurface biogeochemical processes. J Phys Conf Ser 2007;78(1):012063. http://dx.doi.org/10.1088/1742-6596/78/1/012063.

[33] Golfier F, Quintard M, Cherblanc F, Zinn BA, Wood BD. Comparison of theory and experiment for solute transport in highly heterogeneous porous medium. Adv Water Resour 2007;30(11):2235–61. http://dx.doi.org/10.1016/j.advwatres.2011.04.019.

[34] Battiato I, Tartakovsky DM, Tartakovsky AM, Scheibe TD. Hybrid models of reactive transport in porous and fractured media. Adv Water Resour 2011;34(9,SI):1140–50. http://dx.doi.org/10.1016/j.advwatres.2011.01.012.

[35] Rockhold ML, Yarwood RR, Niemet MR, Bottomley PJ, Selker JS. Considerations for modeling bacterial-induced changes in hydraulic properties of variably saturated porous media. Adv Water Resour 2002;25(5):477–95. http://dx.doi.org/10.1016/S0309-1708(02)00023-4.

[36] Wang G, Or D. Aqueous films limit bacterial cell motility and colony expansion on partially saturated rough surfaces. Environ Microbiol 2010;12(5):1363–73. http://dx.doi.org/10.1111/j.1462-2920.2010.02180.x.

[37] Gladkikh M, Bryant S. Prediction of interfacial areas during imbibition in simple porous media. Adv Water Resour 2003;26(6):609–22. http://dx.doi.org/10.1016/S0309-1708(03)00034-4.

[38] Baveye P, Vandevivere P, Hoyle B, DeLeo P, Sanchez de Lozada D. Environmental impact and mechanisms of the biological clogging of saturated soils and aquifer materials. Crit Rev Environ Sci Technol 1998;28(2):123–91. http://dx.doi.org/10.1080/10643389891254197.

[39] Wan J, Wilson J, Kieft T. Influence of the gas–water interface on transport of microorganisms through unsaturated porous media. Appl Environ Microbiol 1994;60(2):509–16.

[40] Southam G, Whitney M, Knickerbocker C. Structural characterization of the hydrocarbon degrading bacteria–oil interface: implications for bioremediation. Int Biodeterior Biodegrad 2001;47(4):197–201. http://dx.doi.org/10.1016/S0964-8305(01)00051-8.

[41] Dorobantu LS, Yeung AKC, Foght JM, Gray MR. Stabilization of oil–water emulsions by hydrophobic bacteria. Appl Environ Microbiol 2004;70(10):6333–6. http://dx.doi.org/10.1128/AEM.70.10.6333-6336.2004.

[42] Dornseiffer P, Meyer B, Heinzle E. Modeling of anaerobic formate kinetics in mixed biofilm culture using dynamic membrane mass spectrometric measurement. Biotechnol Bioeng 1995;45(3):219–28. http://dx.doi.org/10.1002/bit.260450306.

[43] DeLong EF. Microbiology: resolving a methane mystery. Nature 2000;407(6804):577–9. http://dx.doi.org/10.1038/35036677.

[44] Boetius A, Ravenschlag K, Schubert CJ, Rickert D, Widdel F, Gieseke A, Amann R, Jorgensen BB, Witte U, Pfannkuche O. A marine microbial consortium apparently mediating anaerobic oxidation of methane. Nature 2000;407(6804):623–6.

[45] Orphan VJ, House CH, Hinrichs K-U, McKeegan KD, DeLong EF. Methane-consuming archaea revealed by directly coupled isotopic and phylogenetic analysis. Science 2001;293(5529):484–7. http://dx.doi.org/10.1126/science.1061338.

[46] Alpkvist E, Klapper I. A multidimensional multispecies continuum model for heterogeneous biofilm development. Bull Math Biol 2007;69(2):765–89. http://dx.doi.org/10.1007/s11538-006-9168-7.

[47] NIST thermodynamics source database. In: Linstrom PJ, Mallard WG, editors. NIST chemistry webbook, NIST standard reference database number 69. Gaithersburg MD: National Institute of Standards and Technology; 2013 p. 20899. <http://webbook.nist.gov> [Thermodynamics Research Center, NIST Boulder Laboratories].

[48] Bryers JD. Biofilms II: process analysis and applications. Process engineering. Wiley; 2000. p. 13–44 [chap. 1.2].

[49] Stams A, Elferink S, Westermann P. Metabolic interactions between methanogenic consortia and anaerobic respiring bacteria. In: Ahring B, Angelidaki I, de Macario E, Gavala H, Hofman-Bang J, Macario A, Elferink S, Raskin L, Stams A, Westermann P, Zheng D, editors. Biomethanation I. Advances in biochemical engineering/biotechnology, vol. 81. Berlin/Heidelberg: Springer; 2003, ISBN 978-3-540-44322-3. p. 31–56.

[50] Lovley DR, Dwyer DF, Klug MJ. Kinetic analysis of competition between sulfate reducers and methanogens for hydrogen in sediments. Appl Environ Microbiol 1982;43(6):1373–9.

[51] Goodwin S, Conrad R, Zeikus JG. Influence of pH on microbial hydrogen metabolism in diverse sedimentary ecosystems. Appl Environ Microbiol 1988;54(2):590–3.

[52] Bradley AS, Hayes JM, Summons RE. Extraordinary 13C enrichment of diether lipids at the lost city hydrothermal field indicates a carbon-limited ecosystem. Geochim Cosmochim Acta 2009;73(1):102–18. http://dx.doi.org/10.1016/j.gca.2008.10.005.

[53] Khanal SK. Anaerobic biotechnology for bioenergy production: principles and applications. Oxford, UK: Wiley-Blackwell; 2008.

[54] Kotsyurbenko OR, Glagolev MV, Nozhevnikova AN, Conrad R. Competition between homoacetogenic bacteria and methanogenic archaea for hydrogen at low temperature. FEMS Microbiol Ecol 2001;38(2–3):153–9. http://dx.doi.org/10.1111/j.1574-6941.2001.tb00893.x.

[55] Oude Elferink SJWH, Luppens SBI, Marcelis CLM, Stams AJM. Kinetics of acetate oxidation by two sulfate reducers isolated from anaerobic granular sludge. Appl Environ Microbiol 1998;64(6):2301–3.

[56] Scholten JC, van Bodegom PM, Vogelaar J, van Ittersum A, Hordijk K, Roelofsen W, Stams AJ. Effect of sulfate and nitrate on acetate conversion by anaerobic microorganisms in a freshwater sediment. FEMS Microbiol Ecol 2002;42(3):375–85. http://dx.doi.org/10.1111/j.1574-6941.2002.tb01027.x.

[57] Husain A. Mathematical models of the kinetics of anaerobic digestio—a selected review. Biomass Bioenergy 1998;14(5–6):561–71. http://dx.doi.org/10.1016/S0961-9534(97)10047-2.

[58] Kacem M, Salvador S, Quintard M. Textural characterization of media composed of compacted pieces of cardboard and polyethylene using a gas tracer method. Waste Manage 2009;29:660–7. http://dx.doi.org/10.1016/j.wasman.2008.09.002.

[59] Helmig R, Class H, Huber R, Sheta H, Ewing R, Hinkelmann R, Jakobs H, Bastian P. Architecture of the modular program system MUFTE-UG for simulating multiphase flow and transport processes in heterogeneous porous media. Math Geol 1998;2:123–31.

[60] Duan Z, Mller N, Greenberg J, Weare JH. The prediction of methane solubility in natural waters to high ionic strength from 0 to 250 °C and from 0 to 1600 bar. Geochim Cosmochim Acta 1992;56(4):1451–60. http://dx.doi.org/10.1016/0016-7037(92)90215-5.

[61] Duan Z, Sun R. An improved model calculating CO_2 solubility in pure water and aqueous NaCl solutions from 273 to 533 K and from 0 to 2000 bar. Chem Geol 2003;193(3–4):257–71. http://dx.doi.org/10.1016/S0009-2541(02)00263-2.

[62] Jáuregui-Haza UJ, Pardillo-Fontdevila EJ, Wilhelm AM, Delmas H. Solubility of hydrogen and carbon monoxide in water and some organic solvents. Latin Am Appl Res 2004;34:71–4.

[63] Fairbanks DF, Wilke CR. Diffusion coefficients in multicomponent gas mixtures. Ind Eng Chem 1950;42(3):471–5. http://dx.doi.org/10.1021/ie50483a022.

[64] Fuller EN, Schettler PD, Giddings JC. New method for prediction of binary gas-phase diffusion coefficients. Ind Eng Chem 1966;58(5):18–27. http://dx.doi.org/10.1021/ie50677a007.

[65] Stewart PS. Diffusion in biofilms. J Bacteriol 2003;185(5):1485–91. http://dx.doi.org/10.1128/JB.185.5.1485-1491.2003.

[66] Zhang TC, Bishop PL. Density, porosity, and pore structure of biofilms. Water Res 1994;28(11):2267–77. http://dx.doi.org/10.1016/0043-1354(94)90042-6.